Draft version February 2, 2008
Preprint typeset using LaTeX style emulateapj v. 11/12/01

SPECTRAL FEATURES IN THE THERMAL EMISSION FROM ISOLATED NEUTRON STARS: DEPENDENCE ON MAGNETIC FIELD STRENGTHS

Wynn C. G. Ho[1] and Dong Lai
Center for Radiophysics and Space Research, Department of Astronomy, Cornell University, Ithaca, NY 14853
wynnho, dong@astro.cornell.edu
Draft version February 2, 2008

ABSTRACT

We study several effects that influence the strength of the proton cyclotron and atomic features in the thermal spectra of magnetic neutron stars. We show that it is possible for vacuum polarization to strongly suppress the spectral lines when the magnetic field $B \gtrsim 10^{14}$ G. For weaker fields ($B \lesssim 7 \times 10^{13}$ G), the surface spectrum is unaffected by vacuum polarization; thus the proton cyclotron absorption line can have a large equivalent width. Using an approximate calculation of the synthetic spectra, we show that variation of magnetic fields over the neutron star surface leads to broadening of the line. The recently detected absorption features from the isolated neutron stars RX J1308.6 + 2127, RX J1605.3 + 3249, and RX J0720.4 − 3125 can plausibly be explained by the proton cyclotron resonance, with possible blending due to atomic transitions, in the atmosphere of the star.

Subject headings: line: formation — magnetic fields — stars: atmospheres — stars: magnetic fields — stars: neutron — X-rays: stars

1. INTRODUCTION

In the last few years, considerable observational resources (e.g., *Chandra* and *XMM-Newton* telescopes) have been devoted to the study of thermal emission from isolated neutron stars (NSs) and, in particular, to the search for spectral features in the radiation. For many NSs, the spectra are found to be featureless and often well fit by a blackbody (e.g., Marshall & Schulz 2002; Burwitz et al. 2003; see Pavlov, Zavlin, & Sanwal 2002 for a review).

Recently, absorption features have been found in the thermal emission of several isolated NSs. For example, the spectrum of the young NS 1E 1207.4 − 5209 (with surface temperature $T_{\rm eff} \simeq 2$ MK) shows features at 0.7 and 1.4 keV (Sanwal et al. 2002; Mereghetti et al. 2002; Hailey & Mori 2002) and possibly at 2.1 and 2.8 keV (Bignami et al. 2003). Two NSs, RX J1308.6 + 2127 (= RBS 1223) and RX J1605.3 + 3249, belonging to the class of dim, radio-quiet isolated NSs (see Haberl 2003), have been observed to possess broad absorption features in their spectra: at $\simeq 0.2 - 0.3$ keV for RX J1308.6 + 2127 (Haberl et al. 2003a) and at $\simeq 0.45$ keV for RX J1605.3 + 3249 (van Kerkwijk et al. 2004). These are in contrast to two similar dim NSs, RX J1856.5 − 3754 (Pons et al. 2002; Burwitz et al. 2003) and RX J0720.4 − 3125 (Paerels et al. 2001), which show featureless, blackbody-like spectra (however, see Haberl et al. 2003b for the detection of a line at 0.27 keV in RX J0720.4 − 3125). It is particularly striking that, although RX J0720.4 − 3125, RX J1605.3 + 3249, and RX J1308.6 + 2127 have similar effective temperatures ($\simeq$ 1 MK), the equivalent widths (EW) of their lines are very different (van Kerkwijk 2003), from weakest in RX J0720.4 − 3125 (EW $\approx$ 40 eV) to stronger in RX J1605.3 + 3249 (EW $\approx$ 80 eV) to the strongest in RX J1308.6 + 2127 (EW $\approx$ 150 eV). Motivated by these observations, we study in this paper the strength of the proton cyclotron line (and atomic lines) in the atmosphere emission of NSs as a function of magnetic field strength. We show that the absorption features observed in the three NSs (RX J1308.6 + 2127, RX J1605.3 + 3249, RX J0720.4 − 3125) can possibly be explained by the proton cyclotron resonance at (unredshifted) energy

$$E_{Bp} = \frac{\hbar e B}{m_p c} = 0.63\, B_{14}\ \text{keV}, \qquad (1)$$

where $B = 10^{14} B_{14}$ G is the magnetic field strength. (There may be blending of absorption features from radiative transitions in neutral H atoms). We also show that, owing to the vacuum polarization effect, the EW of the line can decrease dramatically as the magnetic field enters the magnetar regime ($B \gtrsim 10^{14}$ G).

In §2, we review and elaborate upon the effect of vacuum polarization on radiative transfer in NS atmospheres. In §3, we present our numerical results for the atmosphere spectra with different magnetic field strengths; these results illustrate the suppression of atmosphere line features as the field strength increases. We consider synthetic spectra from NS atmospheres in §4 and discuss our results in §5.

2. VACUUM POLARIZATION EFFECT ON RADIATIVE TRANSFER IN NEUTRON STAR ATMOSPHERES

Before presenting our numerical results of NS atmospheric spectra for different magnetic field strengths (§3), we first review and elaborate upon the key physics of the vacuum polarization effect on radiative transfer in strong magnetic fields (see Lai & Ho 2002, Ho & Lai 2003, hereafter LH02, HL03; see especially §2 of Lai & Ho 2003a, hereafter LH03).

2.1. *Mode Conversion: Two Magnetic Field Regimes*

Quantum electrodynamics predicts that in strong magnetic fields the vacuum becomes birefringent. In a magnetized NS atmosphere, both the plasma and vacuum

[1] Current address: Kavli Institute for Particle Astrophysics and Cosmology, Stanford University/Stanford Linear Accelerator Center, P.O. Box 20450, Mail Stop 29, Stanford, CA, 94309

polarizations contribute to the dielectric property of the medium. A "vacuum resonance" arises when these two contributions "compensate" each other (Gnedin, Pavlov, & Shibanov 1978; Mészáros & Ventura 1979; Pavlov & Shibanov 1979; Ventura, Nagel, & Mészáros 1979). For a photon of energy E, the vacuum resonance occurs at the density

$$\rho_{\rm V} \simeq 0.964\, Y_e^{-1} B_{14}^2 E_1^2 f^{-2}\ {\rm g\ cm^{-3}}, \tag{2}$$

where Y_e is the electron fraction, $E_1 = E/(1\ {\rm keV})$, and $f = f(B)$ is a slowly varying function of B and is of order unity (LH02; HL03). For $\rho > \rho_{\rm V}$ (where the plasma effect dominates the dielectric tensor) and $\rho < \rho_{\rm V}$ (where vacuum polarization dominates), the photon modes (for $E \ll E_{Be} = 1.16\, B_{14}$ MeV, the electron cyclotron energy) are almost linearly polarized: the extraordinary mode (X-mode) has its electric field vector perpendicular to the $\hat{\mathbf{k}}$-$\hat{\mathbf{B}}$ plane, while the ordinary mode (O-mode) is polarized along the $\hat{\mathbf{k}}$-$\hat{\mathbf{B}}$ plane (where $\hat{\mathbf{k}}$ specifies the direction of photon propagation and $\hat{\mathbf{B}}$ is the unit vector along the magnetic field). Near $\rho = \rho_{\rm V}$, however, the normal modes become circularly polarized as a result of the "cancellation" of the plasma and vacuum effects. When a photon propagates outward in the NS atmosphere, its polarization state will evolve adiabatically if the density variation is sufficiently gentle. Thus, a X-mode (O-mode) photon will be converted into a O-mode (X-mode) as it traverses the vacuum resonance. For this conversion to be effective, the adiabatic condition must be satisfied:

$$E \gtrsim E_{\rm ad} = 2.55 \left(f\, \tan\theta_{kB} |1-u_{\rm i}|\right)^{2/3} \left(\frac{1\,{\rm cm}}{H_\rho}\right)^{1/3}\ {\rm keV}, \tag{3}$$

where θ_{kB} is the angle between $\hat{\mathbf{k}}$ and $\hat{\mathbf{B}}$, $u_{\rm i} = (E_{Bp}/E)^2$, and $H_\rho = |dz/d\ln\rho|$ is the density scale height (evaluated at $\rho = \rho_{\rm V}$) along the ray. For an ionized hydrogen atmosphere, $H_\rho \simeq 2kT/(m_p g\cos\theta) = 1.65\, T_6/(g_{14}\cos\theta)$ cm, where $T = 10^6\, T_6$ K is the temperature, $g = 10^{14} g_{14}$ cm s^{-2} is the gravitational acceleration, and θ is the angle between the ray and the surface normal. In general, the mode conversion probability is given by $P_{\rm con} = 1 - e^{-(\pi/2)(E/E_{\rm ad})^3}$.

Because the two photon modes have very different opacities, the vacuum polarization-induced mode conversion can significantly affect radiative transfer in magnetized atmospheres. When the vacuum polarization effect is neglected (nv), the decoupling densities of the O-mode and X-mode photons (i.e., the densities of their respective photospheres) are approximately given by (see LH02)

$$\rho_{\rm O,nv} \approx 0.42\, T_6^{-1/4} E_1^{3/2} S^{-1/2}\ {\rm g\ cm^{-3}} \tag{4}$$

$$\rho_{\rm X,nv} \approx 486\, T_6^{-1/4} E_1^{1/2} S^{-1/2} B_{14}\ {\rm g\ cm^{-3}}, \tag{5}$$

where $S = 1 - e^{-E/kT}$. Thus the X-mode photons are produced in deeper, hotter layers in the atmosphere than the O-mode photons. When vacuum polarization is taken into account, the decoupling densities can be altered depending on the location of the vacuum resonance $\rho_{\rm V}$ relative to $\rho_{\rm O,nv}$ and $\rho_{\rm X,nv}$ (see Fig. 1). For "normal" magnetic fields,

$$B < B_l \approx 6.6\times 10^{13}\, T_6^{-1/8} E_1^{-1/4} S^{-1/4}\ {\rm G},^2 \tag{6}$$

the vacuum resonance lies outside both photospheres ($\rho_{\rm V} < \rho_{\rm O,nv} < \rho_{\rm X,nv}$); for the magnetar field regime, $B > B_l$, the vacuum resonance lies between these two photospheres ($\rho_{\rm O,nv} < \rho_{\rm V} < \rho_{\rm X,nv}$). These two field regimes correspond to qualitatively different vacuum polarization effects on the radiative transfer.

We can estimate the effective decoupling (photosphere) densities of the two photon modes when mode conversion at the vacuum resonance is taken into account (see, e.g., LH02). Consider first the "normal" field regime $B < B_l$. The free-free opacities of the two modes are approximately given by (neglecting angle-dependent factors) $\kappa_{\rm O} \simeq 9.3\,\rho_1 T_6^{-1/2} E_1^{-3} S$ cm^{2}g^{-1} and $\kappa_{\rm X} \simeq \kappa_{\rm O} u_{\rm e}^{-1}$, where $\rho = \rho_1\,{\rm g\ cm^{-3}}$ and $u_{\rm e} = (E_{Be}/E)^2 \gg 1$. From hydrostatic equilibrium, the column density y at density ρ is $y = 0.83\,\rho_1 T_6$ g cm^{-2} (for $g_{14} = 2$). The column depth of the X-mode photosphere is determined by $\int_{y_{\rm V}}^{y_{\rm X}} \kappa_{\rm X} dy + \int_0^{y_{\rm V}} \kappa_{\rm O} dy = 2/3$. Thus the photosphere density of the X-mode photons (which convert to the O-mode upon traversing the vacuum resonance) is

$$\begin{aligned}\rho_{\rm X\to O} &\simeq \left[\rho_{\rm X,nv}^2 + \rho_{\rm V}(1-u_{\rm e})\right]^{1/2} \\ &\simeq \rho_{\rm X,nv}\left[1-(B/B_l)^4\right]^{1/2}.\end{aligned} \tag{7}$$

Similarly, the photosphere density of the O-mode photons (which convert to the X-mode at the resonance) is

$$\rho_{\rm O\to X} \simeq \rho_{\rm O,nv}\left[1+(B/B_l)^4\right]^{1/2}. \tag{8}$$

Thus, when $(B/B_l)^4 \ll 1$, the photospheres of the two modes are given by equations (4) and (5), and there is no net change in the total emission spectrum. We note, however, that the X-ray polarization signals are dramatically affected by vacuum polarization in this "normal" field regime (see Lai & Ho 2003b).

For the magnetar field regime, we find that the effective photosphere densities are given by

$$\rho_{\rm O\to X} \simeq \rho_{\rm V}\left[1+(B_l/B)^4\right]^{1/2} \tag{9}$$

$$\rho_{\rm X\to O} \simeq \rho_{\rm O,nv}. \tag{10}$$

Thus for $(B/B_l)^4 \gg 1$, the O-mode photosphere is unchanged by vacuum polarization, while the X-mode photons (which carry the bulk of the flux) emerge from the vacuum resonance layers. We expect that the total spectrum will be affected by vacuum polarization in this regime (see §3).

2.2. *No Mode Conversion*

The numerical results shown in §3 are based on the "full mode conversion" ansatz, i.e., when we treat the vacuum polarization effect, mode conversion is assumed for all photon energies and directions of propagation. In reality, mode conversion is complete only when the adiabatic condition is satisfied [see eq. (3)]. A proper treatment of partial mode conversion in radiative transfer requires solving the Stokes parameters of the radiation field, rather than the intensities of the two photon modes (see LH03). The current generation of NS atmosphere models cannot properly treat partial mode conversion. We note

[2] Since B_l depends weakly on T, one may use $T_{\rm eff}/(10^6\ {\rm K})$ as an estimate for T_6. They only differ by a factor of a few in the cases considered here.

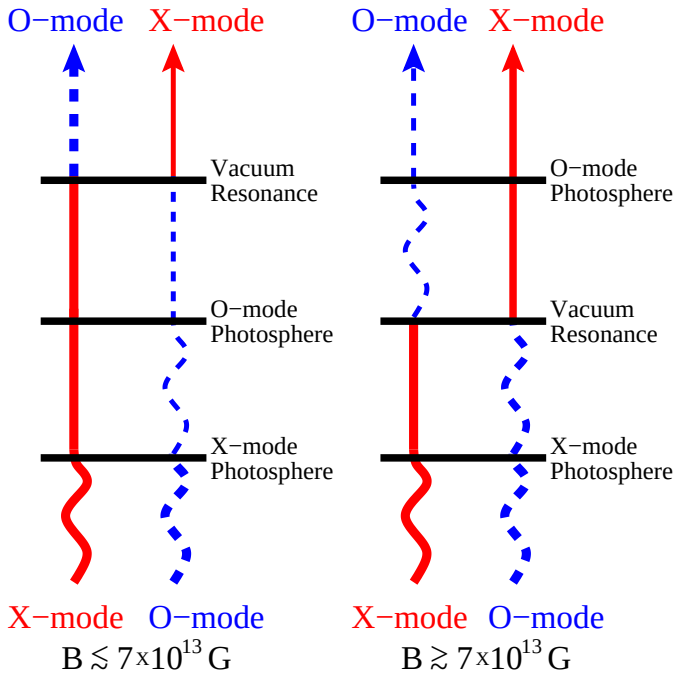

FIG. 1.— A schematic diagram illustrating how vacuum polarization-induced mode conversion affects the emergent radiation from a magnetized NS atmosphere. The photosphere is defined by where the optical depth (measured from the surface) is 2/3 and is where the photon decouples from the matter. The left side applies to the "normal" field regime [$B \lesssim 7\times10^{13}$ G; see eq. (6)], in which the vacuum resonance lies outside the photospheres of the two modes. The right side applies to the "superstrong" field regime ($B \gtrsim 7\times10^{13}$ G), in which the vacuum resonance lies between the two photospheres.

that, in the opposite limit (i.e., the complete non-adiabatic limit or when mode conversion at the vacuum resonance is turned off), the X-mode photon decoupling depth can still be affected by vacuum polarization. This is because the X-mode opacity (without mode conversion) exhibits a sharp rise near the resonance. As a result, the X-mode decoupling density is close to $\rho_{\rm V}$ for sufficiently high photon energies (see LH02 and HL03). As discussed in §4 of HL03, the proton cyclotron line can be suppressed even in the non-adiabatic limit, when the magnetic field is in the range a few $\times\ 10^{14}$ G $\lesssim Bf^{-4/5}T_6^{1/10} \lesssim 2\times10^{15}$ G. (This range of magnetic fields is very approximate since they depend on the direction of photon propagation and redistribution of photon spectral flux occurs in real atmospheres.)

By assuming full mode conversion in §3, we are artificially exaggerating the vacuum polarization effect on the emergent spectrum; despite this, we expect the trend (i.e., the magnetic field dependence of the spectral features) described in §3 to be correct (see HL03 for a comparison of numerical results based on the "full mode conversion" ansatz and the "no conversion" ansatz). Most importantly, near the ion cyclotron energy ($u_{\rm i} \approx 1$), the adiabatic condition is always satisfied [see eq. (3); see especially Fig. 6 of LH03]. For example, at $B = 7\times10^{13}$ G ($E_{Bp} = 0.44$ keV), the adiabatic condition is satisfied when $E > 0.40$ keV and $E > 0.42$ keV for $\theta_{kB} = 15°$ and 30°, respectively; at $B = 10^{14}$ G ($E_{Bp} = 0.63$ keV), eq. (3) is satisfied when $E > 0.54$ keV and $E > 0.58$ keV for $\theta_{kB} = 15°$ and 30°, respectively. Thus we expect the mode conversion calculation to be more accurate.

3. ATMOSPHERE SPECTRA: DEPENDENCE ON MAGNETIC FIELD STRENGTH

Figures 2-4 depict the spectra of ionized hydrogen atmospheres for different field strengths, all with $T_{\rm eff} = 10^6$ K and the magnetic field perpendicular to the stellar surface. These correspond to emission from a local patch on the NS surface and are calculated using atmosphere models in radiative equilibrium (see Ho & Lai 2001 and HL03 for details). When the vacuum polarization effect is neglected (see the curves labeled "no vp"), all spectra exhibit a broad absorption feature due to the proton cyclotron resonance (Ho & Lai 2001; cf. Zane et al. 2001; Lloyd 2003). When the vacuum polarization effect is included, the spectra for different field strengths can be very different. For $B = 4\times10^{13}$ G, vacuum polarization produces no measurable difference in the spectrum (see Fig. 2), although we note that the vacuum effect increases the temperature of the atmosphere layers outside the photospheres of both photon modes (see HL03). For $B = 10^{14}$ G (see Fig. 4), which satisfies $(B/B_l)^4 \gg 1$, the effective X-mode photosphere is located at the vacuum resonance density where mode conversion takes place [$\rho_{\rm O\to X} \simeq \rho_{\rm V}$; see eq. (9)]. Since the X-mode photons (which carry the bulk of the thermal energy) emerge from shallower layers of the atmosphere (compared to the no vacuum polarization case), the high-energy spectral tail is softened, and the spectrum is closer to a blackbody (although the spectrum is still harder than blackbody because of non-grey opacities). Also, for magnetar field strengths, since photons with energies around E_{Bp} (both near the cyclotron line center and outside the line) decouple from similar depths (i.e. at density $\rho_{\rm V}$) in the atmosphere, the proton cyclotron line is suppressed by the vacuum polarization effect (cf. Zane

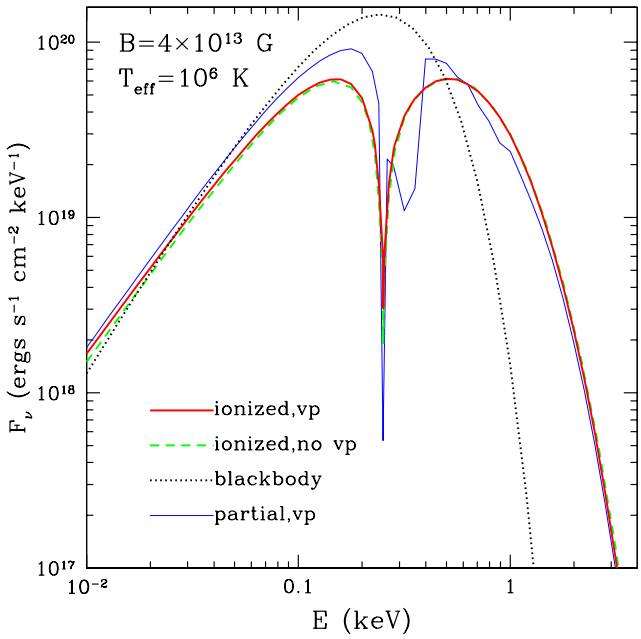

FIG. 2.— Spectra of fully ionized hydrogen atmospheres with $T_{\rm eff} = 10^6$ K and $B = 4 \times 10^{13}$ G. The thick solid line refers to the atmosphere with the vacuum polarization effect included (vp), the dashed line refers to the atmosphere without vacuum polarization (no vp), and the dotted line is for a blackbody with $T = 10^6$ K. The result for a partially ionized atmosphere including vacuum polarization is also shown (thin solid line).

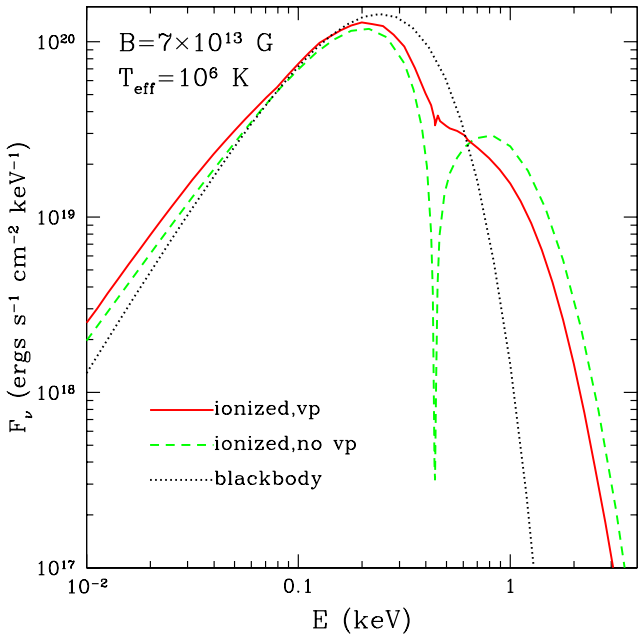

FIG. 3.— Same as Fig. 2, except for $B = 7 \times 10^{13}$ G.

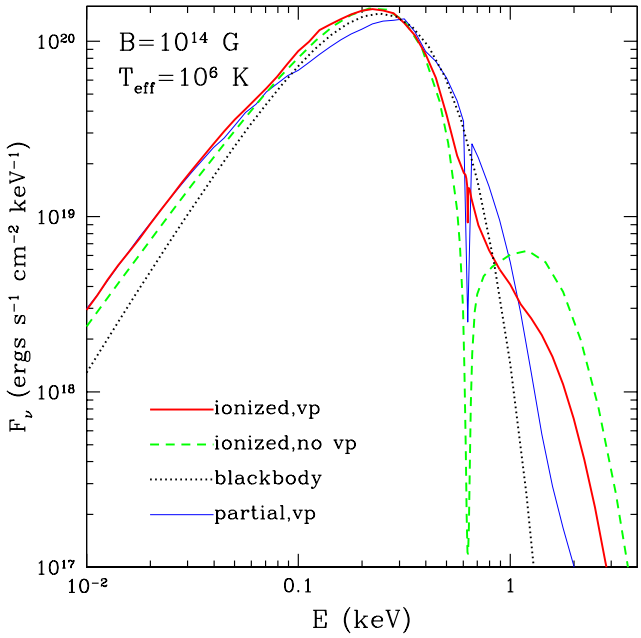

FIG. 4.— Same as Fig. 2, except from $B = 10^{14}$ G.

et al. 2001; Lloyd 2003). We see from Fig. 3 that the $B = 7\times10^{13}$ G case is intermediate between the "normal" field regime and the magnetar field regime.

For the temperature and magnetic field strengths considered in Figs. 2-4, the fraction of neutral H atoms in the atmosphere is not negligible, and atomic bound-bound and bound-free transitions may also give rise to absorption features. However, partially ionized magnetic atmosphere models are not as well developed as fully ionized models (see Ho et al. 2003). In Figs. 2 and 4, we also show the spectra of partially ionized H models for $B = 4\times10^{13}$ G and $B = 10^{14}$ G, including the effect of vacuum polarization (using the "full mode conversion" ansatz); these are based on the latest opacity and equation of state results for magnetized H plasmas (Potekhin & Chabrier 2003, 2004). For $B = 4\times10^{13}$ G, the absorption feature associated with the ground-state bound-free transition lies at $\simeq 0.44$ keV, and the bound-bound transition (from $s = 0, \nu = 0$ to $s = 1, \nu = 0$) is at 0.35 keV, which is close to the proton cyclotron resonance; these features are unaffected by the vacuum polarization effect. For $B = 10^{14}$ G, the bound-free feature is at 0.54 keV, and the bound-bound transition is at 0.74 keV, which is also close to E_{Bp}. Like the proton cyclotron resonance in the magnetar field regime, these atomic features are also suppressed by the vacuum polarization effect.

The results shown in Figs. 2-4 assume the adiabatic condition is always satisfied [see eq. (3) and §2.2]. Numerical models, with $B \le 10^{14}$ G and $T_{\rm eff} = 10^6$ K and assuming no mode conversion, do not show suppression of the proton cyclotron line since there is negligible photon flux at high energies to be redistributed to lower energies; line suppression (with no mode conversion) starts becoming important at $T_{\rm eff} \approx 3\times10^6$ K for $B \approx 10^{14}$ G (see, e.g., Fig. 8 of Ho et al. 2003). Nevertheless, as discussed in §2.2, we believe the full mode conversion calculation to be more accurate (since the adiabatic condition is always satisfied) near the proton cyclotron energy, and the vacuum polarization-induced line suppression shown here should occur.

4. SYNTHETIC SPECTRA FROM NEUTRON STAR SURFACES

The spectra presented in §3 correspond to emission from a local patch of the NS surface. The proton cyclotron line in the local spectrum exhibits a rather spiky feature, which is clearly not observed (see also Ho & Lai 2001; Zane et al. 2001; Lloyd 2003). To compare with observations, we need to calculate the synthetic spectrum from the whole NS surface. Such synthetic spectra is necessarily model-dependent (see Zane et al. 2001 for a different model and method), as the variations of magnetic field and temperature on the NS surface are unknown.

Here, for illustrative purposes, we assume a dipole magnetic field configuration and consider two models for the temperature variation: (1) a uniform surface temperature over the entire NS surface $T_0(\tau)$; (2) a (somewhat arbitrarily-chosen) non-uniform temperature distribution given by

$$T(\tau,\gamma) = T_{\rm p}(\tau)\cos^2\gamma + T_{\rm eq}(\tau)\sin^2\gamma, \qquad (11)$$

where γ is the magnetic colatitude, $\tau = -\int \rho\kappa_0^{\rm es}\, dr$ is the Thomson depth in the atmosphere, and $\kappa_0^{\rm es}$ is the Thomson opacity. We generate the temperature profiles $T_{\rm p}(\tau)$ and $T_{\rm eq}(\tau)$ from our atmosphere models for effective temperatures $T_{\rm eff}$ and magnetic fields B given by $(T_{\rm eff}, B) = (T_{\rm eff}^{\rm p}, B_{\rm p})$ and $(T_{\rm eff}^{\rm eq}, B_{\rm eq})$, respectively, and we assume $T_0(\tau)$ is the same as $T_{\rm p}(\tau)$.

Let the angle between the line of sight toward the observer (the Z-axis) and the axis of the magnetic pole be Θ. (For a spinning NS, Θ obviously varies as the star rotates.) The observed spectral flux can be calculated using the standard procedure, including general relativistic effects (Pechenick, Ftaclas, & Cohen 1983; see also Pavlov

& Zavlin 2000). At a given local patch on the NS surface, we denote the direction of the photons which enter the detector by $\hat{\mathbf{k}}$; the angle between $\hat{\mathbf{k}}$ and the local surface normal is θ and the azimuthal angle of the emitting patch is ϕ. For a given mode j, we approximate the specific intensity of the radiation from this patch by $B_\nu(T)/2$ (neglecting the correction to the source function due to scattering), where $B_\nu(T)$ is the Planck function and T is the temperature at $\tau_\nu^j(\theta,\phi) = 2/3$. Here, $\tau_\nu^j(\theta,\phi)$ is the effective optical depth along the ray,

$$\tau_\nu^j(\theta,\phi) = \frac{1}{\kappa_0^{\rm es}} \int_0^\tau \left(\kappa_j^{\rm a}\kappa_j^{\rm t}\right)^{1/2} \frac{d\tau'}{\cos\theta}, \tag{12}$$

where $\kappa_j^{\rm a}$ and $\kappa_j^{\rm t}$ are the absorption and total opacities, respectively. Interpolating from a table of calculated optical depths $\tau_\nu^j(\tau,\theta,\phi)$, we determine the value of τ at which $\tau_\nu^j = 2/3$, thereby obtaining the source function for each mode. The observed flux spectrum f_{ν_0} (at the observed frequency ν_0) from the entire NS surface is then $f_{\nu_0} = f_{\nu_0}^{\rm X} + f_{\nu_0}^{\rm O}$, with

$$f_{\nu_0}^j = (1+z)^{-1} \left(\frac{R}{D}\right)^2 \int_0^{2\pi} d\phi \int_0^{\pi/2} d\theta\, \sin\theta\cos\theta\, \frac{B_\nu(\theta,\phi)}{2}, \tag{13}$$

where $(1+z) = (1-2GM/Rc^2)^{-1/2}$ is the redshift factor, $\nu_0 = \nu/(1+z)$ and D is the distance to the source (we assume the NS mass and radius are $M = 1.4M_\odot$ and $R = 10$ km, respectively).

Figure 5 shows the computed synthetic spectra from a fully ionized hydrogen atmosphere with a dipole magnetic field distribution ($B_{\rm p} = 4\times10^{13}$ G) and uniform and non-uniform temperature distributions over the NS surface. The proton cyclotron line at $E_{Bp} = 0.25$ keV for $B = 4\times10^{13}$ G is broadened significantly when the emission is integrated over the entire NS surface due to the variation of the magnetic field: the equivalent widths for the two models shown are ~ 80 and 120 eV, as compared to ~ 130 and 150 eV for models with a constant magnetic field, and the centroid energy shifts by $\sim 10-20\%$ (roughly similar to the low B results of Zane et al. 2001, despite the differences in model and method). The equivalent width of the line is significant, comparable to that of the absorption features observed in the isolated NSs RX J1308.6 + 2127 (Haberl et al. 2003a) and RX J1605.3+3249 (van Kerkwijk et al. 2004) (see §5).

5. DISCUSSION

In several recent papers (Lai & Ho 2002, 2003; Ho & Lai 2003), we have shown that at superstrong magnetic fields, $B \gtrsim 10^{14}$ G, vacuum polarization can significantly affect the radiation spectrum from magnetized neutron star atmospheres: it softens the high-energy tail of the spectrum and suppresses the proton cyclotron feature (above ~ 0.6 keV, unredshifted) and other features (see also Ho et al. 2003). The latter could provide an explanation for the non-detection thus far of lines in the observed thermal spectra of several anomalous X-ray pulsars (Patel et al. 2001, 2003; Juett et al. 2002; Tiengo et al. 2002; Morii et al. 2003) and soft gamma-ray repeaters (Kulkarni et al. 2003), which are thought to possess $B \gtrsim 10^{14}$ G.

In this paper, we have studied the dependence of the neutron star atmosphere spectrum on the magnetic field strength. As we explain qualitatively and show numerically, at normal neutron star magnetic fields, $B \lesssim 10^{14}$ G, vacuum polarization has little effect on the atmosphere emission spectra. Therefore, strong proton cyclotron or other atomic features may be present in the thermal spectrum.

Our calculations of neutron star synthetic spectra, taking into account the line broadening effect due to magnetic field variation over the neutron star surface, show that the recently observed broad absorption features in several dim isolated neutron stars could be explained naturally as the proton cyclotron line (with possible blending from atomic lines of neutral hydrogen) from neutron star atmospheres with $B \lesssim 10^{14}$ G (see Fig. 5). The variation in the strength of the observed spectral features in these sources is then due to different fractions of the surface with $B \lesssim 10^{14}$ G.

For RX J0720.4 − 3125, the weakness (phase-averaged EW $\approx$ 40 eV) of the line at 0.27 keV suggests that most of the observable surface of this neutron star has $B \gtrsim 10^{14}$ G, and the line is from the magnetic equatorial region of the star (where B is weaker). The observed line energy does not change with phase but has a larger EW at pulse decline/minimum (Haberl et al. 2003b), which also indicates the line is produced at a small region near the magnetic equator. Note, however, that Kaplan et al. (2002) and Zane et al. (2002) place an upper limit of $\sim$ a few $\times\, 10^{-13}$s s^{-1} on the period derivative of RX J0720.4 − 3125, which, given its period of 8.39 s, implies a dipole field with $B_{\rm dipole} < 5\times10^{13}$ G; thus our inference of the surface field based on the thermal spectrum implies an appreciable non-dipolar magnetic field on the neutron star.

For RX J1308.6+2127, the stronger (EW $\approx$ 155 eV) line at 0.3 keV suggests that most of the observable surface of this neutron star has $B \lesssim 10^{14}$ G. This neutron star also has a double peaked pulse profile (Haberl et al. 2003a), as compared to the very sinusoidal single peaked pulse profile of RX J0720.4 − 3125 (Haberl et al. 2003b). The difference in pulse profiles may be due to differences in the viewing geometry and angle between the magnetic and rotation axes: in the case of RX J1308.6 + 2127, the observer sees the equatorial region most of the time (thus the stronger line and slightly larger pulse fraction) and each magnetic pole, while only one pole is visible in the case of RX J0720.4 − 3125.

Our calculations show that, for a given line-emitting area, the 0.45 keV line of RX J1605.3 + 3249 should have a smaller EW than the 0.27 keV line of RX J0720.4 − 3125. However, the line is stronger (EW $\approx$ 80 eV) in RX J1605.3 + 3249. One possible way to reconcile the observed smaller EW of the 0.27 keV line in RX J0720.4 − 3125[3] is for the line-emitting area (with $B \lesssim 10^{14}$ G) to be a small fraction of the observed surface, while the larger fraction of the surface has a much higher magnetic field ($B \gtrsim 10^{14}$ G). Alternatively, we have only considered hydrogen, and some of the lines may be due to other elements, such as helium.

As discussed in §2.2, the numerical treatment of the vac-

[3] de Vries et al. (2004) find long-term changes in the spectra of RX J0720.4 − 3125; it is not clear whether this variability can affect the EW of the line.

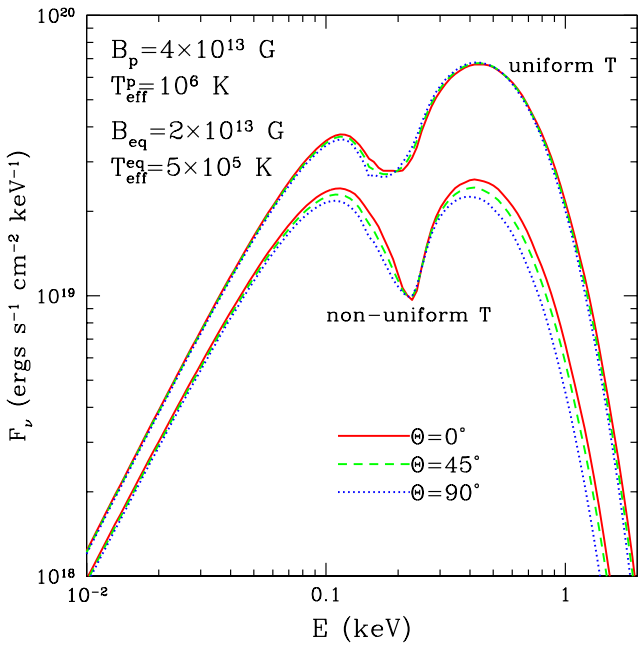

FIG. 5.— Synthetic spectra (unredshifted and with R^2/D^2 factored out) for fully ionized hydrogen atmosphere emission from a NS with a dipole magnetic field distribution and uniform and non-uniform [see eq. (11)] temperature distributions over the NS surface. The uniform temperature spectrum uses the temperature profile constructed from the atmosphere model with $B = 4\times10^{13}$ G and $T_{\rm eff} = 10^6$ K, while the non-uniform temperature spectrum uses the temperature profiles $T_{\rm p}$ and $T_{\rm eq}$ constructed from the atmosphere models with $B = 4\times10^{13}$ G and $T_{\rm eff} = 10^6$ K and $B = 2\times10^{13}$ G and $T_{\rm eff} = 5\times10^5$ K, respectively. Θ is the angle between the observer's line of sight and the magnetic axis.

uum polarization effect in the neutron star atmosphere models is approximate, i.e., it does not properly account for the partial mode conversion associated with the vacuum resonance. Future work in this direction is necessary (see LH03), as well as a more accurate and comprehensive study of partially ionized atmosphere models (see Ho et al. 2003). Furthermore, we have only examined thermal emission; there have been cyclotron features seen in the non-thermal emission from magnetars (e.g., the 5.0 keV feature from SGR 1806 − 20 during outburst, Ibrahim et al. 2002, 2003; the 8.1 keV feature from AXP 1RXS J170849 − 400910, Rea et al. 2003). Such theoretical/numerical studies, when combined with observational data, should provide useful constraints on the nature of various types of neutron stars, including the dim isolated neutron stars.

We thank Alexander Potekhin for supplying the opacity tables of Potekhin & Chabrier (2003), which were used in Figs. 2 and 4 to compute spectra from partially ionized hydrogen atmospheres. We also thank Marten van Kerkwijk for useful discussion. We appreciate the useful suggestions and comments of the anonymous referee. Our computations made use of the facilities at the Cornell Hewitt Computer Laboratory. This work is supported in part by NASA grant NAG 5-12034 and NSF grants AST 9986740 and AST 0307252.

REFERENCES

Bignami, G.F., Caraveo, P.A., De Luca, A., & Mereghetti, S. 2003, Nature, 423, 725
Burwitz, V., Haberl, F., Neuhäuser, R., Predehl, P., Trümper, & Zavlin, V.E. 2003, A&A, 399, 1109
de Vries, C.P., Vink, J., Méndez, M., & Verbunt, F. 2004, A&A, in press (astro-ph/0401028)
Gnedin, Yu.N., Pavlov, G.G., & Shibanov, Yu.A. 1978, Sov. Astron. Lett., 4, 117
Haberl, F. 2003, Adv. Sp. Res., in press (astro-ph/0302540)
Haberl, F., Schwope, A.D., Hambaryan, V., Hasinger, G., & Motch, C. 2003a, A&A, 403, L19
Haberl, F., Zavlin, V.E., Trümper, J., & Burwitz, V. 2003b, A&A, submitted (astro-ph/0312413)
Hailey, C.J. & Mori, K. 2002, ApJL, 578, L133
Ho, W.C.G. & Lai, D. 2001, MNRAS, 327, 1081
Ho, W.C.G. & Lai, D. 2003, MNRAS, 338, 233 (HL03)
Ho, W.C.G., Lai, D., Potekhin, A.Y., & Chabrier, G. 2003, ApJ, 599, 1293
Ibrahim, A.I., Swank, J.H., & Parke, W. 2003, ApJL, 584, L17
Ibrahim, A.I., Safi-Harb, S., Swank, J.H., Parke, W., Zane, S., & Turolla, R. 2002, ApJL, 574, L51
Juett, A.M., Marshall, H.L., Chakrabarty, D., & Schulz, N.S. 2002, ApJL, 568, L31
Kaplan, D.L., Kulkarni, S.R., van Kerkwijk, M.H., & Marshall, H.L. 2002, ApJL, 570, L79
Kulkarni, S.R., Kaplan, D.L., Marshall, H.L., Frail, D.A., Murakami, T., & Yonetoku, D. 2003, ApJ, 585, 948
Lai, D. & Ho, W.C.G. 2002, ApJ, 566, 373 (LH02)
Lai, D. & Ho, W.C.G. 2003a, ApJ, 588, 962 (LH03)
Lai, D. & Ho, W.C.G. 2003b, Phys. Rev. Lett., 91, 071101
Lloyd, D.A. 2003, MNRAS, submitted (astro-ph/0303561)
Marshall, H.L. & Schulz, N.S. 2002, ApJ, 574, 377
Mereghetti, S., De Luca, A., Caraveo, P.A., Becker, W., Mignani, R., & Bignami, G.F. 2002, ApJ, 581, 1280
Mészáros, P. & Ventura, J. 1979, Phys. Rev. D, 19, 3565
Morii, M., Sato, R., Kataoka, J., & Kawai, N. 2003, PASJ, 55, L45
Paerels, F., et al. 2001, A&A, 365, L298
Patel, S.K., et al. 2001, ApJL, 563, L45
Patel, S.K., et al. 2003, ApJ, 587, 367
Pavlov, G.G. & Shibanov, Yu.A. 1979, Sov. Phys. JETP, 49, 741
Pavlov, G.G. & Zavlin, V.E. 2000, ApJ, 529, 1011

Pavlov, G.G., Zavlin, V.E., & Sanwal, D. 2002, in Proc. 270 WE-Heraeus Seminar on Neutron Stars, Pulsars, and Supernova Remnants, eds. Becker, W., Lesch, H., & Trümper, J., (MPE Rep. 278; Garching: MPI), p.273
Pechenick, K.R., Ftaclas, C., & Cohen, J.M. 1983, ApJ, 274, 846
Pons, J.A., Walter, F.M., Lattimer, J.M., Prakash, M., Neuhäuser, R., & An, P. 2002, ApJ, 564, 981
Potekhin, A.Y. & Chabrier, G. 2003, ApJ, 585, 955
Potekhin, A.Y. & Chabrier, G. 2004, ApJ, 600, 317
Rea, N., Israel, G.L., Stella, L., Oosterbroek, T., Mereghetti, S., Angelini, L., Campana, S., & Covino, S. 2003, ApJL, 586, L65
Sanwal, D., Pavlov, G.G., Zavlin, V.E., & Teter, M.A. 2002, ApJL, 574, L61
Tiengo, A., Goehler, E., Staubert, R., & Mereghetti, S. 2002, A&A, 383, 182
van Kerkwijk, M.H. 2003, in Young Neutron Stars and Their Environments, eds. Camilo, F. & Gaensler, B. (IAU Symp. 218), in press (astro-ph/0310389)
van Kerkwijk, M.H., Kaplan, D.L., Durant, M., Kulkarni, S.R., Paerels, F. 2004, ApJ, submitted
Ventura, J., Nagel, W., & Mészáros, P. 1979, ApJL, 233, L125
Zane, S., Turolla, R., Stella, L., & Treves, A. 2001, ApJ, 560, 384
Zane, S., Haberl, F., Cropper, M., Zavlin, V.E., Lumb, D., Sembay, S., & Motch, C. 2002, MNRAS, 334, 345